Modeling Metrology for Calibration of OPC Models

Chris A. Mack[a], Ananthan Raghunathan[b], John Sturtevant[b], Yunfei Deng[b], Christian Zuniga[b], Kostas Adam[b]

[a]Lithoguru.com, 1605 Watchhill Rd, Austin, TX 78703, E-mail: chris@lithoguru.com
[b]Mentor Graphics, Willsonville, OR, 97070

Abstract

Optical Proximity Correction (OPC) has continually improved in accuracy over the years by adding more physically based models. Here, we further extend OPC modeling by adding the Analytical Linescan Model (ALM) to account for systematic biases in CD-SEM metrology. The ALM was added to a conventional OPC model calibration flow and the accuracy of the calibrated model with the ALM was compared to the standard model without the ALM using validation data. Without using any adjustable parameters in the ALM, OPC validation accuracy was improved by 5%. While very preliminary, these results give hope that modeling metrology could be an important next step in OPC model improvement.

Subject Terms: OPC, optical proximity correction, modeling, metrology, analytical linescan model, calibration

1. Introduction

Optical Proximity Correction (OPC) enables low-k_1 lithography by changing the pattern shapes on the mask to correct for the non-linear process of printing those patterns on a wafer. This is a classic and difficult "inverse" problem: given a desired pattern on the wafer for a fixed lithography process, what pattern on the mask will most closely achieve that desired wafer pattern? The difficulty is compounded by that fact that the design of an entire chip, with its billions of features, must be corrected in this way. Today, this inverse problem is solved using compact lithography models run on clusters of hundreds or thousands of microprocessors. The trade-off between speed and accuracy required for these models is severe and unforgiving. Further, continuous improvement is needed since at each technology node, the accuracy needs scale at least with the feature sizes of the device.

The compact lithography models used in OPC have progressed from mostly empirical kernels that are convolved with the design and then thresholded, to much more rigorous and physics-based approaches. There are two important ways that OPC models have become more rigorous: by separating out the rigorous parts from the empirical parts, and by measuring as many physically-based input parameters as possible rather than calibrating them. Thus, physics-based models for optical imaging were separated from the more empirical resist models. Calculations of aerial images became vector calculations of the image in resist. Mask models were separated from the imaging models, and 3D EMF mask models were employed. Actual aberrations, source shapes, and thin-film properties are now measured and supplied as inputs to the model. But more can still be done.

The most empirical part of an OPC model is the resist model. It is there that the three-dimensional world of the actual photoresist is compressed to two dimensions (required for the speed of the calculations). Also, it is in the compact resist model that any and all "left-over" processes not explicitly separated out will be lumped. One such process is metrology. The OPC model and its unknown parameters are calibrated by comparisons of model outputs to CD-SEM measurements made on specific test structures called gauges. By comparing the output of the OPC model to an SEM measurement, the OPC model is implicitly modeling the SEM measurement process in addition to the resist printing process.

A goal of this work is to insert a new metrology model into the OPC model calibration flow, thus continuing the trend towards greater model separability and more physics-based models. The CD-SEM metrology model that we have used is called the analytical linescan model (ALM).[1,2,3] More details of the ALM will be given in the next section. A standard calibrated OPC resist model predicts the resist contour for a given mask pattern (*i.e.*, one of the gauges used

for model calibration). In the new model flow, the ALM is used to predict the CD value that would be obtained if the resist profile was measured in a CD-SEM. This predicted CD-SEM output is then compared to the experimental CD-SEM data and this difference is minimized as a part of the standard calibration. As the experimental work described below will show, the result is a more predictive OPC model.
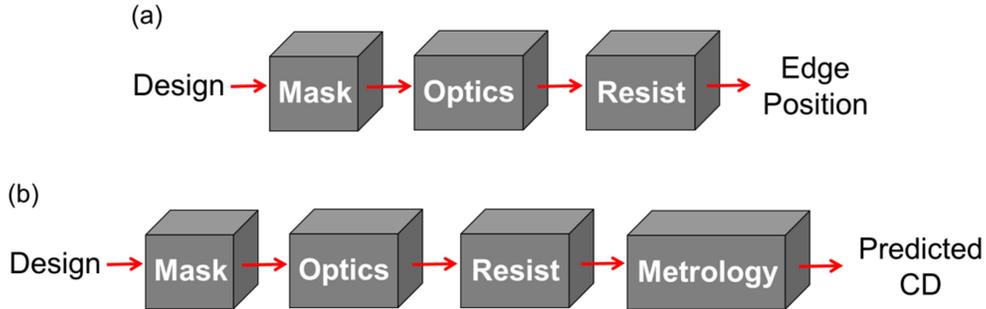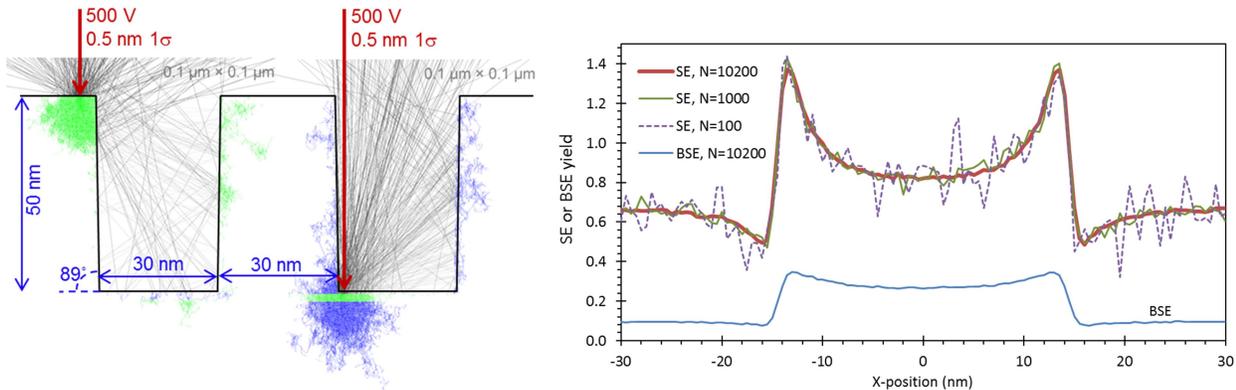

Figure 1. The OPC model as it is currently used has separate resist, optics, and resist models (a). In this work, we separate out the metrology component from the resist model in the calibration flow by creating a separate, physically based model of the CD-SEM measurement process (b).

2. The Analytical Linescan Model

The first step in developing a simplified analytical linescan model is to generate a series of calculated SEM images from known sample structures. Simulations of SEM images were performed using JMONSEL (**J**ava **Mon**te Carlo Simulator of **S**econdary **El**ectrons), a program developed at the National Institute of Standards and Technology (NIST).[4] JMONSEL is used here as a "virtual SEM", where the user can input idealized structures from a limited list of materials, with perfect user-defined geometries. The user can also define SEM parameters such as the number of incident electrons per pixel, pixel size, spot size, and beam energy.

In previous studies,[2,3] the virtual samples consisted of isolated edges (steps) and line/space patterns of various sizes and pitches on a uniform substrate. Features were made of silicon or PMMA (used as a material model for resist) on a planar silicon substrate. The sidewall angle of the edge or feature was varied between 45° and 90°. The height of the feature was varied from below 10 nm to 100 nm, though was focused on the range from 20 – 50 nm. The landing energy was set at 500 eV and a point beam of electrons was used at each pixel location (with the effect of a larger beam size to be included later). An example linescan is shown in Figure 2.
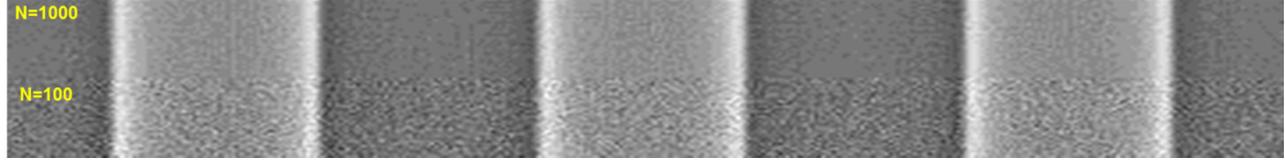
Figure 2. Example outputs from JMONSEL. Top-left: Simulated trajectories in a 30 nm line/space Si-on-thin SiO$_2$ structure at 500 V and 0.5 nm incident spot (one standard deviation Gaussian profile), where the interaction volumes can be seen at feature tops and bottoms. Top-right: Example linescan, including waveforms for secondary electron (SE) and backscatter electron (BSE) yields. SE electrons are defined as having energies ≤ 50 eV, with BSE electrons defined as having energies > 50 eV. Bottom: Simulated image of same waveform for N=1000 (top) and N=100 (bottom). Figure from Ref. 1.

In this work, we extend the analytical linescan model to include the case of resist on organic BARC on silicon. PMMA was used as a material model for an organic BARC. A range of BARC thicknesses were simulated, but it was quickly discovered that a BARC thickness greater than about 20 nm appeared infinitely thick from the perspective of the SEM at 500V. Since in practice organic BARCs always exceed that thickness, the work presented below focused on a 50-nm thick layer of BARC.

A full mathematical description of the ALM can be found in previous publicationsl.[1,2,3] Here, we will focus on the use of the ALM for the case of resist on BARC. The linescan, corresponding to the detected secondary electrons (secondaries), will be $SE(x)$, with $x = 0$ at the edge position and the feature material found at $x > 0$. For an isolated vertical edge (step), we have the following linescan expression for the case of a point incident beam:

$$SE(x) = SE(-\infty)\left[1 - \alpha_f e^{x/\sigma_f} - \alpha_b e^{x/\sigma_b}\right]u(-x) + SE(\infty)\left[1 + \alpha_e e^{-x/\sigma_e} - \alpha_v e^{-x/\sigma_v}\right]u(x) \qquad (1)$$

where $u(x)$ is the unit step function. For the substrate, σ_f and σ_b are the forward and backscatter ranges, respectively, within the substrate material, α_f is the fraction of substrate forward scatter-generated secondaries absorbed by the step, and α_b is the fraction of substrate backscatter-generated secondaries absorbed by the step. When the electron beam is incident on the top of the step, σ_e is the forward scatter range of the step material and α_e is the fraction of those forward-scattered electrons that escape through the edge of the step. When the incident beam is very close to the step, however, the interaction volume of the forward-scattered electrons with the material is reduced, causing the generation of less secondaries. Thus, we subtract a term $\alpha_v e^{-x/\sigma_v}$ to account for this volume loss. $SE(-\infty)$ is the secondary electron signal for the substrate (silicon) a long way from any feature, and $SE(\infty)$ is the secondary electron signal for the top of the step (resist) a long way from the step edge.

For the case of a sloped step, a sloped region of width $h/\tan\theta$ exists between the top and bottom of the step, where θ is the sidewall angle and h is the feature height. If the width of the sloped region is sufficiently large, the middle of the sidewall region has a steady secondary electron signal, which we will call SE_{edge}. This signal level then falls to the bottom level over a characteristic distance δ_1 at the bottom of the step, and rises to the top level over a characteristic distance δ_2 at the top of the step, forming an S-shaped waveform. The model for the linescan in this sloped region is

$$c_1 = SE(-\infty)\left[1 - \alpha_f - \alpha_b\right] - SE_{edge}$$
$$c_2 = SE(+\infty)\left[1 + \alpha_e - \alpha_v\right] - SE_{edge}$$
$$SE(x) = SE_{edge} + \left(c_1 - c_2 e^{-(h/\tan\theta)/\delta_2}\right)e^{-x/\delta_1} + \left(c_2 - c_1 e^{-(h/\tan\theta)/\delta_1}\right)e^{-(h/\tan\theta - x)/\delta_2} \qquad (2)$$

Many of the model parameters used in the above two equations are a function of the sidewall angle, and a few are a function of step height. Letting $\tilde{p}$ represent the value of a parameter p for a 90° step, the variation of the linescan parameters with sidewall angle and feature height for the case of resist on BARC take the forms

$$\sigma_b = s_b h$$

$$\alpha_f = 0.153 + (\tilde{\alpha}_f - 0.153)(1 - \cos\theta)$$

$$\alpha_b = \tilde{\alpha}_b (1 - \cos\theta)^2$$

$$\sigma_e = 3.49 + (\tilde{\sigma}_e - 3.49)(1 - \cos\theta)^2$$

$$\alpha_e = 0.14 + (\tilde{\alpha}_e - 0.14)(1 - \cos\theta)^{1.5}$$

$$\alpha_v = \tilde{\alpha}_v (1 - \cos\theta)^{3.5}$$

$$SE_{edge} = \widetilde{SE}_{edge} \left(1 + 1.33\cos\theta - 4.26\cos^2\theta + 2.82\cos^3\theta\right)$$

$$\delta_1 = 5.15\cos\theta$$

$$\delta_2 = \left(1.6 + \frac{h}{22}\right)\cos\theta$$

(3)

where all dimensions are in nanometers. Further, these equations only apply to the case where $h \geq 20$ nm. The values of the parameters for a 90º sidewall angle are given in Table I.

Table I. Best fit parameters to rigorous Monte Carlo simulations of an isolated PMMA step on a PMMA wafer at 500 V electron landing voltage.

	Resist Step
BARC wafer background signal, $SE(-\infty)$	2.13
BARC wafer forward scatter range, σ_f (nm)	3.5
BARC wafer backscatter range per step height, $s_b = \sigma_b/h$	0.7
BARC wafer forward scatter absorption, $\tilde{\alpha}_f$	0.268
BARC wafer backscatter absorption, $\tilde{\alpha}_b$	0.106
Step sidewall signal, $\widetilde{SE}_{edge}$	3.38
Step forward scatter range, $\tilde{\sigma}_e$ (nm)	3.8
Step volume loss range, σ_v (nm)	1.24
Step edge enhancement factor, $\tilde{\alpha}_e$	2.02
Step volume loss factor, $\tilde{\alpha}_v$	1.2
Step background signal, $SE(\infty)$	2.13

Real scanning electron microscopes do not have point beams of electrons impinging on the sample. Instead, the beam is approximately a Gaussian owing to the finite resolution of the microscope and other beam non-idealities. Thus, the expected linescan will be the point linescan model (equations (1) and (2) combined) convolved with a Gaussian.[2]

A feature such as a line or a space can be constructed as the combination of two edges, using the ALM for an edge defined in the previous section. However, small spaces act as traps for escaping secondary electrons, so that some of the model parameters must be modified as a function of the size of the space. In the region of the space, the result is that smaller spaces have smaller forward scatter absorption and larger backscatter absorption.

$$\alpha_f = \tilde{\alpha}_f \left(1 - e^{-(s/(0.32h))^{0.64}}\right), \quad \alpha_b = \tilde{\alpha}_b \left(1 + 3.0 e^{-(s/h)^{0.6}}\right) \tag{4}$$

where s is the spacewidth. Likewise, when the electron beam scan across the top of the feature, secondaries escaping out of the edge of the feature are more likely to be trapped in the space, causing a reduction in both the step edge enhancement factor and the step volume loss factor.

$$\alpha_e = \tilde{\alpha}_e \left(1 - e^{-(s/(0.46h))^{0.6}}\right), \quad \alpha_v = \tilde{\alpha}_v \left(1 - e^{-(s/(0.26h))^{0.6}}\right) \tag{5}$$

Figure 3 shows an example where are of these factors are taken into account. The ALM prediction matches the Monte Carlo simulations extremely well. And while the example given is for a point beam of electrons, the use of a Gaussian beam incident on the sample does not pose any particular challenges and does not reduce the quality of the match to the Monte Carlo results. It is important to note that the results shown in Figure 3, which are quite typical, do not represent the best fit of the basic ALM model to this one linescan. Such a fit would be even better, with no perceivable differences between the ALM and JMONSEL. Rather, Figure 3 shows the fully parameterized ALM, calibrated across a wide range of resist heights, sidewall angles, feature sizes, and pitches, making an interpolated prediction for just one condition within the entire set used for its calibration.
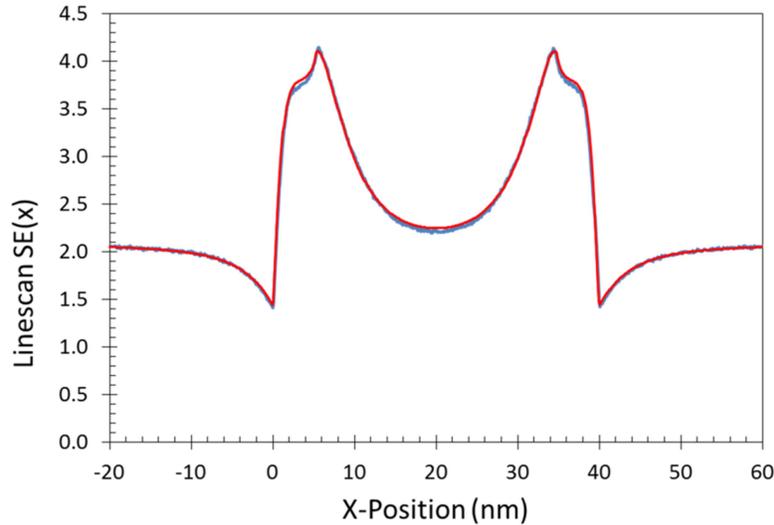

Figure 3. The ALM (red smooth curve) compared to the Monte Carlo simulation results (blue jagged curve) for 50-nm tall resist features on BARC, SWA = 80°, 40-nm lines on a 150-nm pitch. Similar matches are found over a very wide range of feature sizes, pitches, sidewall angles, and resist heights.

3. Adding the ALM to the Calibre OPC Model

The ALM requires as its input a trapezoidal description of the cross-section of the resist pattern being measured. A standard OPC model is quasi-3D and does not predict the resist profile as accurately as a 3D model. Thus, the addition of the ALM is first tested here using a full 3D compact resist model during calibration. Testing of the ALM model using a standard OPC resist model only will be done in future work. The 3D model incorporates 3D resist effects into the optic and resist compact models to accurately simulate resist profiles as shown in Figure 4. The 3D diffusion is modeled by lateral and vertical diffusion and additional resist effects dependent on the height dimension z are included

in the resist model.[5,6] The 3D model gives access to the resist contour at any height z. However, for correction a single resist contour plane is used and the model does not have to be 3D.
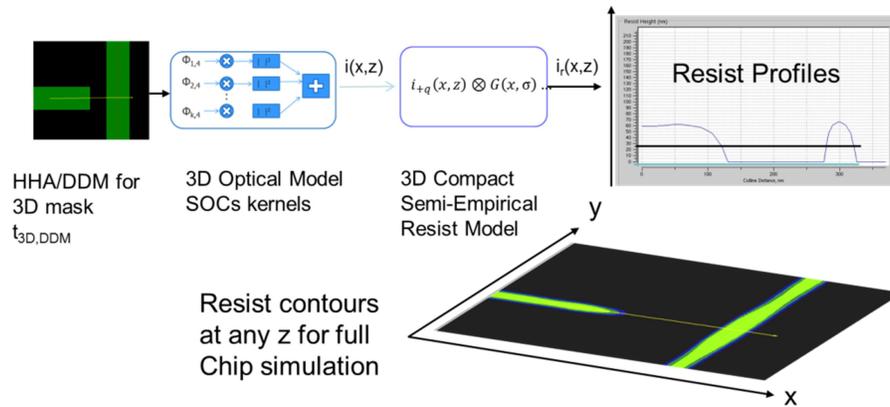

Figure 4. Depiction of the 3D compact semi-empirical resist model used to extract resist profile cross-sections for the ALM.

The resist feature cross-section output of the compact 3D resist model is then fit to a trapezoid. The height of the trapezoid is set to the middle height of the resist model output. The bottom width and sidewall angle of the trapezoid is found by fitting a straight line through the simulated resist profile edge in the region between 20% and 80% of the resist height. While the ALM can handle asymmetric profiles, in the experiment described below all the features were symmetric. Once the best-fit trapezoidal feature was extracted from the simulated 3D profile cross-section, that trapezoid was fed into the ALM for simulation of the measured CD. A simple threshold model was used to extract the CD from the outside edges of the linescan. A baseline signal level was set to be the SE signal at the center of the space. The peak signal was then found, and the CD measured at the indicated fraction level between the baseline and the peak.

The standard OPC flow is shown in Figure 5.[7,8] This flow includes model calibration based upon CD-SEM measurements on training patterns, and subsequent validation on unique patterns not used in the calibration. The test mask contained 221 different 1D features, mostly line/space patterns of various linewidths and pitches, but also two-line patterns as well. These patterns were printed using a commercial 22-nm node metal1 process through dose and focus. Critical dimensions were measured using a CD-SEM operating at 500V. . Besides 221 measured values at best focus and dose, measurements were over a standard range of focus and exposure for a total of 728 measurements (gauges).
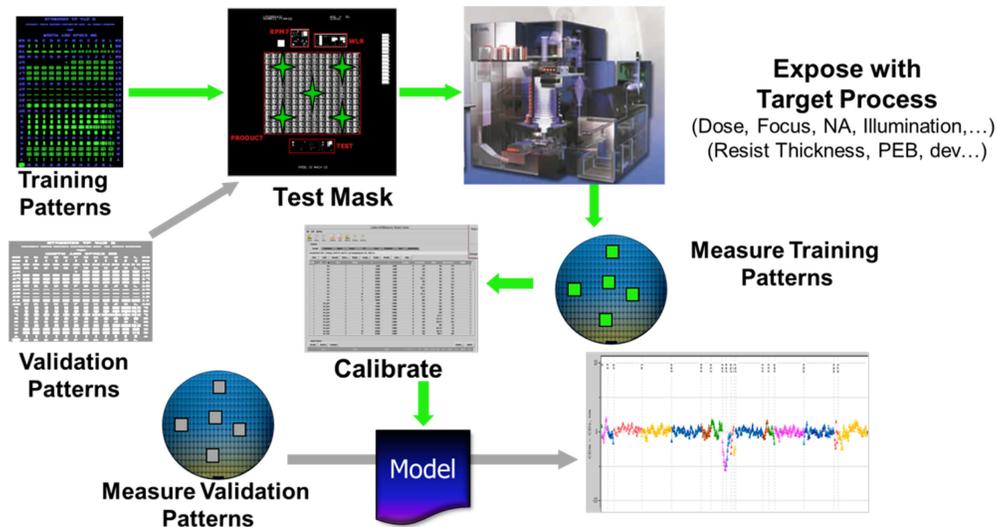
Figure 5. A standard OPC model calibration flow was followed when calibrating the OPC model with and without the ALM included.

The predictability of the ALM was assessed using a common validation procedure. The 728 gauge sample was stratified into a best dose/focus sample and an off-dose/focus sample. Each group was then randomly divided in half. One half of the gauges were then used to calibrate the OPC model with the ALM, and the same gauges were used to calibrate the OPC without the ALM (that is, in its normal configuration). The RMS difference between the model and the CD measurements was used a metric of calibration success, with 1.2 nm being a typical number. Then, using the calibrated model, the second half of the gauges were simulated as a verification data set, and the RMS difference between the model and the CD measurements was used a metric of verification success, with 2.5 nm being a typical number. When using the ALM, no attempt to adjust or calibrate the ALM parameters (Table 1) was made. The threshold value for CD extraction from the ALM linescan was however varied from 0.3 to 0.7.

This random split of the data into a calibration half and a validation half was repeated 25 times. The average of the 25 RMS calibration values and the average of the 25 RMS validation values are shown in Figure 6. The bars show the percent difference of the model with the ALM included as compared to the plan of record (POR), the model without the ALM. A positive value indicates the ALM performed better than the POR, resulting in a lower average RMS value.
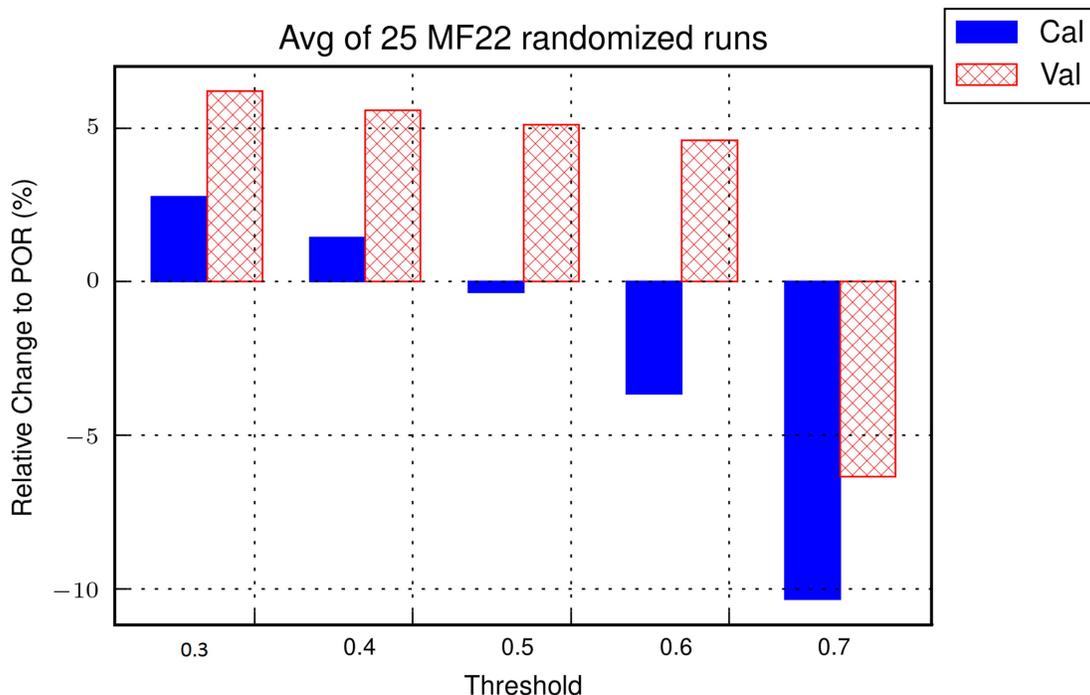
Figure 6. The average of 25 calibration and validation runs are shown as the percent difference of the OPC model with the ALM added to the POR (plan of record use of OPC without the ALM) as a function of the CD measurement threshold. A positive value means the results with the ALM were better (had lower average RMS value) than the POR.

The results shown in Figure 6 show some interesting trends. First, the ALM provides a small improvement (about 5%) to the validation RMS value for most of the threshold values. This indicates that while the ALM does deliver improved predictive capability, the standard OPC resist model in fact does capture most of the metrology effects found in the data. Unlike the validation results, the calibration results show a strong dependence on the CD extraction threshold value. The reason for this dependence is still under investigation. Finally, both the calibration and validation results are worse when the threshold value reaches 0.7. At this high threshold value, the measurement of CD from the linescan becomes unstable as the measurement moves off the part of the signal that shows a steep rise and onto a flatter part of the signal that exists for sloped sidewalls (see Figure 3).

4. Conclusions and Future Work

We have extended the previously published analytical linescan model for the case of an organic photoresist on organic BARC layer, and calibrated ALM parameters to JMONSEL simulated linescans. That ALM was then used in a standard OPC model calibration and validation cycle, and the results compared to a conventional flow without the ALM. Since the empirical compact resist model is known to fit a wide variety of smooth monotonic functions, it was anticipated that the standard flow can already fit to some extent the proximity effect of the CD-SEM. This was shown to be the case, but use of the ALM nonetheless resulted in approximately a 5% improvement in predictive capability for an ensemble of 1D gauges at nominal and through process window conditions. This is a very important result, as it demonstrates that a model of CD-SEM behavior can be incorporated into the OPC model flow, where the goal is to accurately ascribe various effects properly to the originating modules, whether mask, optics, resist, etch, or now metrology.

In future work, we will extend this model to include 2D cases such as contact holes and line ends, as well as fine tune the ALM to represent more complex profiles.

5. Acknowledgements

We would like to thank John Villarrubia of NIST for his writing and continued support of the JMONSEL SEM simulator code, and Ben Bunday of SUNY Poly SEMATECH for running the JMONSEL simulations of resist on BARC used to calibrate the ALM for this study. We would like to thank Todd Bailey and Ramya Viswanathan from GLOBALFOUNDRIES for access to the modeling testcase.

6. References

[1] Benjamin D. Bunday and Chris A. Mack, "Influence of Metrology Error in Measurement of Line Edge Roughness Power Spectral Density", *Metrology, Inspection, and Process Control for Microlithography XXVIII, Proc*., SPIE Vol. **9050**, 90500G (2014).

[2] Chris A. Mack and Benjamin D. Bunday, "Analytical Linescan Model for SEM Metrology", *Metrology, Inspection, and Process Control for Microlithography XXIX*, Proc., SPIE Vol. 9424 (2015) p. 94240F.

[3] Chris A. Mack and Benjamin D. Bunday, "Improvement to the Analytical Linescan Model for SEM Metrology", *Metrology, Inspection, and Process Control for Microlithography XXX, Proc.,* SPIE Vol. 9778 (2016), in press.

[4] J. S. Villarrubia, A. E. Vladár, B. Ming, et al., "Scanning electron microscope measurement of width and shape of 10 nm patterned lines using a JMONSEL-modeled library", *Ultramicroscopy*, **154**, 15 (2015).

[5] Y. Granik, *et al*., "Towards standard process models for OPC", *Proc. SPIE* 6520, 652043 (2007).

[6] Christian Zuniga and Yunfei Deng "Resist toploss and profile modeling for optical proximity correction applications", *J. Micro/Nanolith. MEMS MOEMS*, **13**(4), 043010, (2014).

[7] Chen Ao, *et al*., "Evaluation of compact models for negative tone development layers at 20/14nm nodes", *Proc. SPIE* 9426, 94261P (2015).

[8] John L. Sturtevant, "The evolution of patterning process models in computational lithography", *Advances in Resist Materials and Processing Technology XXVII, Proc.,* SPIE Vol. 7639, 763902 (2011).